AI-Driven Battery-Free Wireless Sensing of Hazardous Liquid Spills via a Frequency-Selective Surface in a Monostatic Antenna Configuration

Pau Casacuberta, *Graduate Student Member, IEEE*, Fatemeh Niknahad, *Graduate Student Member, IEEE*, Ali Maleki Gargari, Ferran Martín, *Fellow, IEEE*, and Mohammad H. Zarifi, *Senior Member, IEEE*

***Abstract*—The detection of spills is paramount in safeguarding safety and mitigating environmental risks in sensitive environments, including laboratories and industrial facilities. Here, the novel artificial intelligence (AI)-driven, battery-free, and wireless sensing methodology are presented for detecting liquid spills using a monostatic wireless sensing system. The system consists of a frequency-selective surface (FSS) serving as the sensor, in conjunction with a horn antenna that functions as the readout equipment. The sensing structure features a 25 × 25 resonator array with a 7-mm periodicity, operating at a resonant frequency of 7.2 GHz. The system analyzes the renormalized S_{11} response to quantify variations caused by the presence of liquid on the FSS, demonstrating a high sensitivity to isopropyl alcohol (IPA) spills. Using machine learning techniques, the framework generates 512 × 512 pixel masks delineating the affected area on the FSS, achieving an $F1$-score exceeding 0.85 for spill localization. This sensing methodology shows potential for integration with augmented reality (AR) systems, enabling enhanced situational awareness and real-time spill localization. Future work aims to enhance the system's capability to detect more hazardous materials and accurately classify them.**

***Index Terms*—Artificial intelligence (AI), deep learning, frequency-selective surface (FSS), laboratory safety, remote monitoring, spill detection, U-Net, wireless sensing.**

I. Introduction

HAZARDOUS liquid spill detection in laboratories and industrial facilities faces challenges: contact-based methods risk exposure, battery-powered systems require maintenance, and vision-based approaches struggle with transparent substances. These limitations necessitate innovative solutions for continuous, intervention-free monitoring.

Artificial intelligence (AI)-enhanced sensing systems have advanced sensor technologies [1], energy harvesting, and AI integration [2] to improve efficiency and precision. Machine learning enhances sensor functionalities [3], achieving a 94% success rate in differentiating water from ethanol [4]. AI-driven techniques promise battery-free applications, highlighting sustainability and adaptability [5].

Frequency-selective surface (FSS)-based sensors show potential in spill detection, achieving good sensitivity for xylene [6]. These systems offer noninvasive, battery-free, passive monitoring, ideal for laboratories or industrial settings. Related innovations include batteryless wireless sensor networks [7] and dual-resonance microstrip antenna for liquid sensing in noisy environments [8].

Addressing the challenge of precise spill localization without complex antenna arrays, we propose a novel battery-free wireless sensing framework using an FSS and a single antenna in a monostatic configuration. The significance of our approach lies in its simplicity, cost-effectiveness, and ability to create accurate spatial masks of affected areas using renormalized S_{11} parameters and deep learning. This represents a substantial advancement for laboratory safety and is compatible with AR integration [9], [10], improving hazardous environment monitoring.

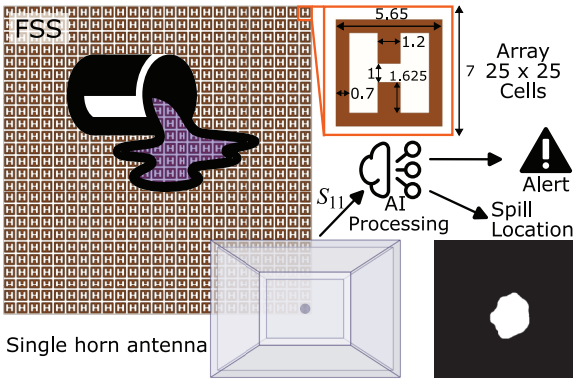

Fig. 1. Example implementation of the setup (top view) showing the FSS cell with dimensions in millimeters, and the relative position of the antenna to the sensing surface. The FSS is fabricated using a chemical etching process on a Rogers RO4350 substrate with a relative permittivity of 3.48, a loss tangent of 0.003, and a thickness of 0.25 mm.

II. System Overview

The setup features an FSS with electric-*LC* resonators tuned to 7.2 GHz and a ground plane (Fig. 1). The FSS

Received 3 February 2025; revised 18 March 2025; accepted 26 March 2025. This work was supported in part by the Ministerio de Ciencia e Innovación (MCIN)/Agencia Estatal de Investigación (AEI) 10.13039/501100011033, Spain, under Project PID2022-139181OB-I00 (ERDF EU); and in part by the Agència de Gestió d'Ajuts Universitaris i de Recerca (AGAUR), Catalonia Government, under Project 2021SGR00192 and Project 2024 ICREA 00114. The work of Pau Casacuberta was supported by the Ministerio de Universidades, Spain, under Grant FPU20/05700. *(Corresponding author: Pau Casacuberta.)*

Pau Casacuberta and Ferran Martín are with CIMITEC, Departament d'Enginyeria Electrònica Universitat Autònoma de Barcelona, 08193 Bellaterra, Spain (e-mail: pau.casacuberta@uab.cat).

Fatemeh Niknahad, Ali Maleki Gargari, and Mohammad H. Zarifi are with the OMEGA Laboratory, University of British Columbia Okanagan, Kelowna, BC V1V 1V7, Canada.

Digital Object Identifier 10.1109/LMWT.2025.3556170

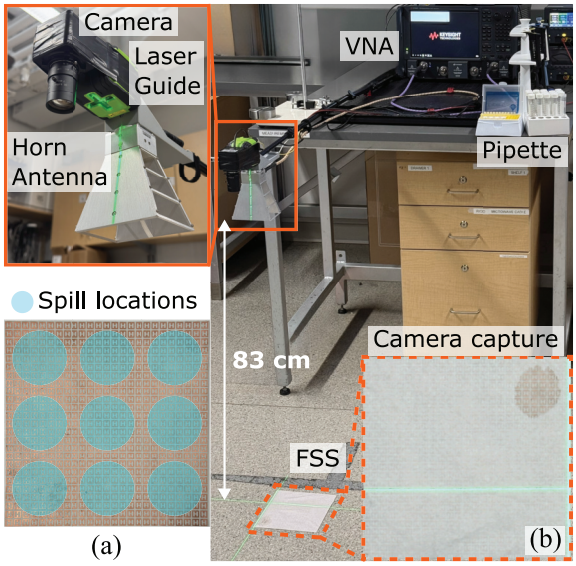

Fig. 2. Experimental setup prepared for IPA spill localizations, along with (a) bare FSS showing spill locations and (b) sample image for model training.

unit cell dimensions were optimized via HFSS simulations for a 7.2-GHz resonance, balancing sensitivity, and fabrication constraints. Extensive optimization was skipped as the FSS's angled position shifts resonance. A wideband A-INFO LB-20180-SF horn antenna is placed 83 cm away, forming a monostatic configuration.

The antenna measures the reflected signal, expressed as the S_{11} response. Two measurements are taken: $S_{11,\text{meas}}$ with the FSS (and potential spill), and $S_{11,\text{env}}$ without the FSS. These are processed using the following equation, as described in [11]:

$$S_{11} = \frac{S_{11,\text{meas}} - S_{11,\text{env}}}{1 - S_{11,\text{meas}} S_{11,\text{env}}}. \quad (1)$$

This enhances sensitivity to FSS response changes by compensating for environmental effects. Experiments used IPA as the liquid under test (LUT). Detection relies on the LUT's dielectric properties, which shift the FSS's resonant frequency, altering the reflected signal to identify the LUT's location.

Data for S_{11} was acquired using a Keysight N5222B VNA from 7 to 7.5 GHz with 2001 frequency points at −5-dBm power, chosen to validate detection with limited spectral data for cost-effective implementation. Measurements were taken every 2 s using Keysight's PNA Data Logger, while an ELP USB 4K camera captured the spill area every 10 s (Fig. 2). A GK011DG laser level precisely positioned the FSS, minimizing symmetry effects. Spills were created by dispensing 100-μL IPA at various locations [Fig. 2(b)], creating realistic patterns across FSS cells.

III. Data Acquisition and Ground-Truth Generation

To streamline dataset generation, spill images were captured with a *Kimiwipe* cloth on the FSS to enhance visibility without affecting RF response [Fig. 2(a)]. These images were processed with Meta's SAM 2.1 AI model [12] to create ground-truth masks. Masks were interpolated between 10-s image intervals to align with 2-s RF measurements. Automation allowed extensive dataset creation, vital for robust machine learning models. This method also enables customized datasets for specific environments, optimizing models for particular scenarios. In rare cases (<1% of images), automatic detection failed, requiring manual annotation. Each image was linked with the associated renormalized S_{11} measurement. We collected 1800 measurements, with 700 nonspill and 1100 spill instances across ten positions, enabling effective model training.

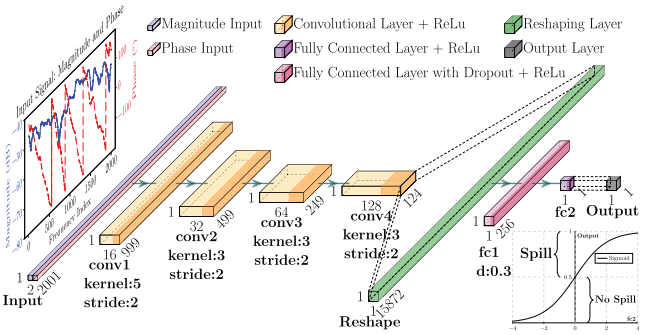

Fig. 3. Spill detection model architecture illustrating the network characteristics, along with an example of input data and binary output after the sigmoid activation function for the last node: "spill" or "no spill."

IV. Model Design

Two machine learning models were constructed that are as follows.

1) *Spill Detection Model:* A CNN determines spill presence using renormalized S_{11} data, with four 1-D convolutional layers followed by two fully connected layers. Convolutional layers recognize trends in magnitude and phase data, while fully connected layers support binary classification. A 0.3 dropout reduces overfitting, see Fig. 3.
2) *Spill Localization Model:* This model forecasts spill distribution using S_{11} magnitude and phase. It begins with a three-layer feature extractor, followed by fully connected layers, culminating in a shallow U-Net with an upscaler for 512×512 resolution masks. The U-Net adapts to processed RF data, acquiring spatial features from frequency response. The initial 1-D CNN extracts frequency features, transformed for U-Net input. The upscaler provides high-resolution output for spill location, see Fig. 4.

V. Training and Evaluation Approaches

The network was trained using PyTorch. The architecture evolved iteratively, balancing efficiency and accuracy through adjustments in filter size and layer count. We performed 100 trials using *Optuna* [13] to optimize training hyperparameters for each model. For the classification model, we refined the learning rate (η) and weight decay (d) associated with the AdamW optimizer, as well as the alpha (α) and gamma (γ) parameters of the focal loss function, thereby incentivizing or penalizing positive and negative outputs. We employed 20-fold cross validation for generalization during training. Similarly, for the localization model, we optimized parameters, including focal loss for all mask points, using fivefold cross validation to achieve robust, dataset-independent hyperparameters. Evaluations were conducted using three approaches.

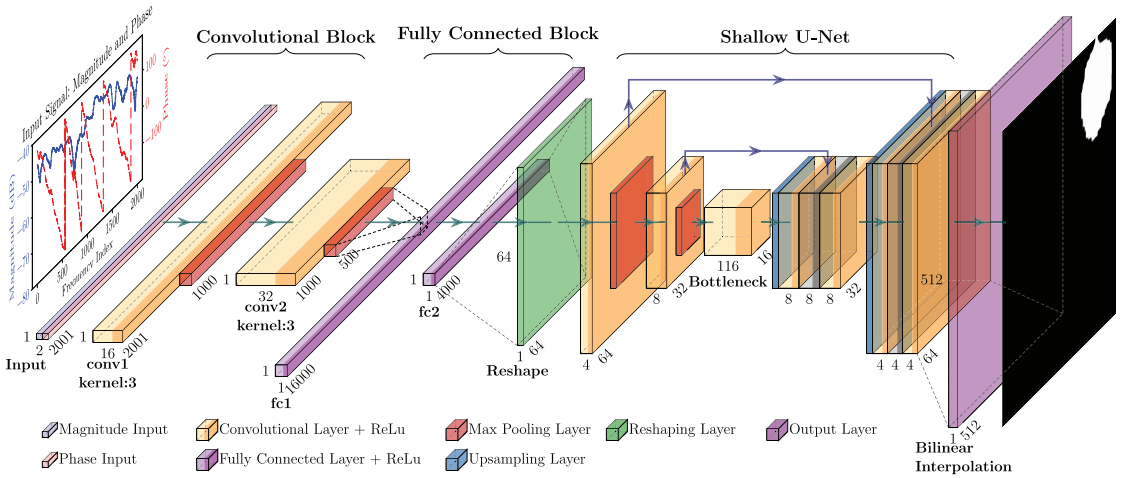

Fig. 4. Spill localization model architecture showcasing the network structure, an example of input data, the corresponding mask output, and various block groups that compose the model.

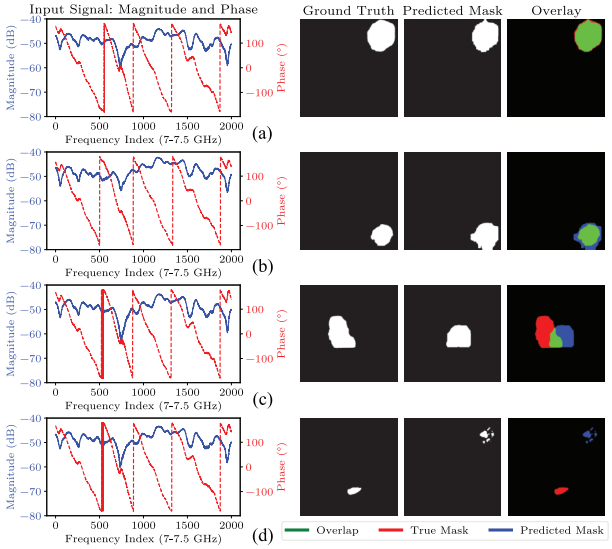

Fig. 5. Results from processing RF data with the localization model: the first column shows the input data, the second displays camera-based and mask-processed training data, and spills are highlighted in white. The third presents the model's raw output and the fourth overlays camera and model outputs. (a)-(b) Correct predictions, (c) partial match, and (d) wrong prediction due to low-volume spill.

1) *Spill Detection Evaluation:* The model achieved an $F1$-score of 0.89, with hyperparameters $\eta = 8.39 \times 10^{-4}$, $d = 4.04 \times 10^{-4}$, $\alpha = 0.21$, and $\gamma = 1.85$.
2) *Spill Localization Evaluation:* We used a balanced dataset by excluding 80% of nonspillage instances, reducing dataset size to focus on spill events. The model obtained an $F1$-score of 0.80, with hyperparameters $\eta = 4.09 \times 10^{-4}$, $d = 2.10 \times 10^{-6}$, $\alpha = 0.98$, and $\gamma = 2.03$.
3) *Application-Oriented Approach:* We used the detection model to filter positive spill cases before applying the localization model. The smaller detection model can operate continuously with less power, activating the localization model only when needed. This approach provided an $F1$-score of 0.85, with hyperparameters $\eta = 7.44 \times 10^{-5}$, $d = 1.37 \times 10^{-5}$, $\alpha = 0.58$, and $\gamma = 1.84$.

VI. Results and Discussion

The proposed methodology identified spills and quantified affected regions using only RF S_{11} measurements. The detection model achieved 83.3% accuracy on 165 test images, correctly identifying 138 cases. With a recall of 96.6%, it missed only 3.4% of actual spills, prioritizing safety by minimizing false negatives. Despite some false positives, the model achieved an F1-score of 89%. The localization model achieved an F1-score of 85%, the overlap measure between predicted and actual spill areas. The average intersection over union between predicted and ground-truth masks was 74% and a mean accuracy of 83.2%, indicating considerable agreement.

Fig. 5 presents some specific results of the localization model. Fig. 5(a) and (b) shows correctly identified spills in two locations, demonstrating the model's localization capabilities. Fig. 5(c) presents a marginal case, where the prediction lacked precision but had some overlap, and the general location was correct. Fig. 5(d) shows a misidentification due to weak RF changes from small spills, indicating a need for additional training data to improve sensitivity for low-volume spills.

VII. Conclusion

We presented a battery-free wireless FSS-based sensing system for spill detection using a monostatic antenna configuration. The proposed system addresses some limitations of traditional vision-based methods, which struggle to detect transparent hazardous liquids due to a lack of contrast with the background. By leveraging RF signals sensitive to permittivity changes, our solution achieved an 85% $F1$-score for localizing transparent liquids like IPA. Future research will explore more AI models, such as recurrent networks, to handle complex spill dynamics and incorporate time-based measurements to aid material classification. The implementation of autonomous systems for detecting, localizing, and identifying spills, combined with AR interfaces, represents a significant advancement toward intelligent safety management in hazardous environments.

Acknowledgment

The authors acknowledge the Syilx Okanagan Nation for their land, where this research was conducted. They thank Rogers Corporation, Chandler, AZ, USA, for substrate support.

REFERENCES

[1] F. Martín and E. Bronchalo Eds.,, *Coupled Structures for Microwave Sensing* (Lecture Notes in Electrical Engineering). Cham, Switzerland: Springer, Jan. 2024, vol. 1150.

[2] N. Wu et al., "AI-enhanced integrated sensing and communications: Advancements, challenges, and prospects," *IEEE Commun. Mag.*, vol. 62, no. 9, pp. 144–150, Sep. 2024.

[3] Y. Zhou, J. Yong, J. Peng, P. Li, M. Tong, and Y. Zhang, "Deep learning-based recognizing liquids using a multi-resonance microwave sensor," in *Proc. Photon. Electromagn. Res. Symp. (PIERS)*, Apr. 2024, pp. 1–8.

[4] K. Colegrave, M. C. Jain, O. Niksan, and M. Zarifi, "Artificial neural networks for antenna-based contactless liquid classification," in *Proc. Int. Conf. Electr., Comput. Energy Technol. (ICECET)*, Jul. 2022, pp. 1–5.

[5] M. Li et al., "Artificial intelligence enabled self-powered wireless sensing for smart industry," *Chem. Eng. J.*, vol. 492, Jul. 2024, Art. no. 152417.

[6] P. M. Njogu, B. Sanz-Izquierdo, and E. A. Parker, "A liquid sensor based on frequency selective surfaces," *IEEE Trans. Antennas Propag.*, vol. 71, no. 1, pp. 631–638, Jan. 2023.

[7] H. M. E. Hussein, M. Rinaldi, M. Onabajo, and C. Cassella, "A chip-less and battery-less subharmonic tag for wireless sensing with parametrically enhanced sensitivity and dynamic range," *Sci. Rep.*, vol. 11, no. 1, p. 3782, Feb. 2021.

[8] L. Zhu, N. Alsaab, M. M. Cheng, and P.-Y. Chen, "A zero-power ubiquitous wireless liquid-level sensor based on microfluidic-integrated microstrip antenna," *IEEE J. Radio Freq. Identificat.*, vol. 4, no. 3, pp. 265–274, Sep. 2020.

[9] V. Balasubramanian and M. H. Zarifi, "Augmented reality-assisted battery-less microwave-based sensors for smart health monitoring of coatings," in *IEEE MTT-S Int. Microw. Symp. Dig.*, Jun. 2024, pp. 277–280.

[10] V. Balasubramanian, O. Niksan, M. C. Jain, K. Golovin, and M. H. Zarifi, "Augmented reality-enhanced microwave-based wireless monitoring system for smart coating applications," *IEEE Trans. Microw. Theory Techn.*, early access, May 30, 2024, doi: 10.1109/TMTT.2024.3403838.

[11] A. Maleki Gargari, M. H. Zarifi, and L. Markley, "Passive matched mushroom structure for a high sensitivity low profile antenna-based material detection system," *IEEE Sensors J.*, vol. 19, no. 15, pp. 6154–6162, Aug. 2019.

[12] N. Ravi et al., "SAM 2: Segment anything in images and videos," 2024, *arXiv:2408.00714*.

[13] T. Akiba, S. Sano, T. Yanase, T. Ohta, and M. Koyama, "Optuna: A next-generation hyperparameter optimization framework," in *Proc. 25th ACM SIGKDD Int. Conf. Knowl. Disc. Data Min.*, 2019, pp. 2623–2631.